

Enhancing light absorption for organic solar cells using front ITO nanograting and back ultrathin Al layer

Li Zhang(张力), Wei-Ning Liu(刘卫宁), Yan-Zhou Wang(王艳周), Qi-Ming Liu(刘奇明), Jun-Shuai Li(栗军帅), Ya-Li Li(李亚丽), and De-Yan He(贺德衍)

Citation: Chin. Phys. B, 2021, 30 (**10**): 104207. DOI: 10.1088/1674-1056/abe92c
Journal homepage: http://cpb.iphy.ac.cn; http://iopscience.iop.org/cpb

What follows is a list of articles you may be interested in

Bound states in the continuum on perfect conducting reflection gratings

Jianfeng Huang(黄剑峰), Qianju Song(宋前举), Peng Hu(胡鹏), Hong Xiang(向红), and Dezhuan Han(韩德专)
Chin. Phys. B, 2021, 30 (**8**): 084211. DOI: 10.1088/1674-1056/abeee4

Dual-function beam splitter of high contrast gratings

Wen-Jing Fang(房文敬), Xin-Ye Fan(范鑫烨), Hui-Juan Niu(牛慧娟), Xia Zhang (张霞), Heng-Ying Xu(许恒迎), and Cheng-Lin Bai(白成林)
Chin. Phys. B, 2021, 30 (**4**): 044205. DOI: 10.1088/1674-1056/abd68d

Broadband absorption enhancement with ultrathin MoS_2 film in the visible regime

Jun Wu(吴俊)
Chin. Phys. B, 2021, 30 (**2**): 024208. DOI: 10.1088/1674-1056/abc3b5

Polarization-independent silicon photonic grating coupler for large spatial light spots

Lijun Yang(杨丽君), Xiaoyan Hu(胡小燕), Bin Li(李斌), and Jing Cao(曹静)
Chin. Phys. B, 2021, 30 (**2**): 024206. DOI: 10.1088/1674-1056/abbc00

Tunable dual-band terahertz graphene absorber with guided mode resonances

Jun Wu(吴俊), Xia-Yin Liu(刘夏吟), and Zhe Huang(黄喆)
Chin. Phys. B, 2021, 30 (**1**): 014202. DOI: 10.1088/1674-1056/abaee2

Enhancing light absorption for organic solar cells using front ITO nanograting and back ultrathin Al layer*

Li Zhang(张力)[1,2,†], Wei-Ning Liu(刘卫宁)[1,2,†], Yan-Zhou Wang(王艳周)[1,2], Qi-Ming Liu(刘奇明)[1,2], Jun-Shuai Li(栗军帅)[1,2,3,‡], Ya-Li Li(李亚丽)[1,2,§], and De-Yan He(贺德衍)[1,2,3]

[1] *Key Laboratory of Special Function Materials & Structure Design of the Ministry of Education, Lanzhou University, Lanzhou* 730000, *China*

[2] *School of Physical Science & Technology, Lanzhou University, Lanzhou* 730000, *China*

[3] *School of Materials & Energy, Lanzhou University, Lanzhou* 730000, *China*

(Received 26 January 2021; revised manuscript received 17 February 2021; accepted manuscript online 24 February 2021)

To address the discrepancy between carrier collection and light absorption of organic solar cells caused by the limited carrier mobility and optical absorption coefficient for the normally employed organic photoactive layers, a light management structure composed of a front indium tin oxide (ITO) nanograting and ultrathin Al layer inserted in between the photoactive layer and the electron transport layer (ETL) is introduced. Owing to the antireflection and light scattering induced by the ITO nanograting and the suppression of light absorption in the ETL by the inserted Al layer, the light absorption of the photoactive layer is significantly enhanced in a spectral range from 400 nm to 650 nm that also covers the main energy region of solar irradiation for the normally employed active materials such as the P3HT:PC_{61}BM blend. The simulation results indicate that comparing with the control device with a planar configuration of ITO/PEDOT:PSS/P3HT:PC_{61}BM (80-nm thick)/ZnO/Al, the short-circuit current density and power conversion efficiency of the optimized light management structure can be improved by 32.86% and 34.46%. Moreover, good omnidirectional light management is observed for the proposed device structure. Owing to the fact that the light management structure possesses the simple structure and excellent performance, the exploration of such a structure can be believed to be significant in fabricating the thin film-based optoelectronic devices.

Keywords: light management structures, ITO nanograting, organic solar cells, thin film-based optoelectronic devices

PACS: 42.79.Dj, 88.40.jr **DOI:** 10.1088/1674-1056/abe92c

1. Introduction

Organic solar cells (OSCs) have attracted a great deal of attention because of the potential advantages including low cost, light weight, mechanical flexibility, and easy-to-implement large-scale and roll-to-roll fabrication.[1–5] To date, power conversion efficiency (PCE) of single junction OSCs has surpassed 18% due to the massive efforts made in various respects from materials to device configurations.[6] However, the gap of the comprehensive performance including PCE, lifetime between OSCs and their inorganic counterparts such as silicon wafer solar cells is still evident.[7–9]

For most of OSCs, the discrepancy between limited carrier mobility and absorption coefficient is the main factor limiting their PCE improvement.[10] How to simultaneously ensure the effective collection of photogenerated carriers and efficient light absorption has become an important scientific issue, which therefore has attracted people to conduct the research in various aspects from the optimization of device configurations to the development of novel materials.[11,12] Among the diverse schemes, incorporating an appropriate light management structure is an effective way of improving light absorption without increasing the thickness of the photoactive layers, and thus has been developed into one of the frontiers. It has been suggested that various antireflection structures,[13–18] photonic crystals,[19–24] metallic nanoparticles,[25–30] and gratings[31–36] be used to enhance light absorption of the relevant devices. However, it is notable that the balance between light absorption enhancement and complexity of the light management structures should be seriously taken into consideration for solar cell applications.

In this study, a simple and high-performance light management structure consisting of an indium tin oxide (ITO) nanograting on the front surface and ultrathin Al layer inserted in between the photoactive layer and the electron transport layer (ETL) is proposed. The combination of antireflection and light scattering by the ITO nanograting leads the light absorption of the photoactive layer to increase remarkably. Moreover, the ultrathin Al layer can suppress the light absorp-

*Project supported by the Natural Science Foundation of Gansu Province, China (Grant No. 20JR10RA611) and the Fundamental Research Funds for Central Universities, China (Grant Nos. lzujbky-2017-178 and lzujbky-2017-181).

†These authors contributed equally to this work.

‡Corresponding author. E-mail: jshli@lzu.edu.cn

§Corresponding author. E-mail: liyli@lzu.edu.cn

© 2021 Chinese Physical Society and IOP Publishing Ltd

tion in the ETL and thus reduce the corresponding energy loss. The simulation results indicate that the short-circuit current density (J_{sc}) and PCE can increase 32.86% and 34.46%, respectively, after incorporating the optimized light management structure into the device with an 80-nm-thick P3HT:PC_{61}BM blend active layer. Moreover, the light management structure exhibits good omnidirectional light management that is expected in solar cell applications.

2. Experiment

Figure 1(a) shows the schematic diagram of the three-dimensional (3D) structure of the investigated device that consists of a front ITO nanograting of 160 nm in the total thickness ($H_1 = H_2 = 80$ nm), a 10-nm thick PEDOT:PSS hole transport layer, an 80-nm thick P3HT:PC_{61}BM photoactive layer, an ultrathin Al layer, a 10-nm thick ZnO ETL, and a 100-nm thick bottom Al layer. As marked in Fig. 1, the ITO layers are arranged periodically (period of P) into a nanograting, in which the width of bottom part (L_1) is larger than the width of top part of the nanograting L_2 (*i.e.*, $L_1 > L_2$), and the thickness of the ultrathin Al layer is denoted as T. The optical properties of the device are investigated by solving the Maxwell's equations through using a finite-difference time-domain method. Since the sunlight can be divided into any pair of mutually perpendicular linear polarization states without a fixed phase relationship, two polarization states with the electric field parallel and perpendicular to the nanograting are adopted in this investigation. Considering the bandgap energy of ~ 1.9 eV for the P3HT:PC_{61}BM blend[37] and the main energy region of the solar irradiation, the optical behaviors are studied in the spectral range of 300 nm–800 nm.

For building the structure for simulation and saving the calculation resource and time as well, periodic boundary conditions are applied to the unit, *i.e.*, the cuboid-shaped box with red edges as exhibited in Fig. 1(b), along the x and y directions. Meanwhile, the perfectly matched layer boundaries are imposed on the top and bottom bounds of the unit, and a monitor is placed above the top bound to determine the light reflection, $R(\lambda)$. The absorption of the photoactive layer at a certain wavelength, denoted by $A(\lambda)$, can be directly extracted from the following equation after the electric field has been calculated:[38]

$$A(\lambda)=\omega\varepsilon_0 \int |E(x,y,z,\omega)|^2 n(\omega)k(\omega)\,\mathrm{d}V, \tag{1}$$

where ω is the angular frequency of the incident light, ε is the permittivity of vacuum, E is the local electric-field strength in the photoactive layer, n and k represent the real and imaginary parts of the P3HT:PC_{61}BM refractive index, respectively. Based on Eq. (1), the short-circuit current density (J_{sc}) of the devices from the following equation:

$$J_{sc} = e \int \frac{\lambda}{h} \cdot A(\lambda) \cdot I_{AM1.5G}(\lambda)\,\mathrm{d}\lambda, \tag{2}$$

where e is a unit charge, h is the Planck constant, and $I_{AM\ 1.5G}$ (λ) is the spectrum of the energy flux density at AM 1.5G illumination. And moreover, to make a quantitative comparison of light trapping capability among the devices, the integrated reflectance ($R_{in.}$) is calculated using the following equation:[39]

$$R_{in.} = \frac{\int R(\lambda) \cdot I_{AM\ 1.5G}(\lambda)\,\mathrm{d}\lambda}{\int I_{AM\ 1.5G}(\lambda)\,\mathrm{d}\lambda}, \tag{3}$$

the integration range is from 300 nm to 652.6 nm, corresponding to the bandgap energy of the P3HT:PC_{61}BM blend.

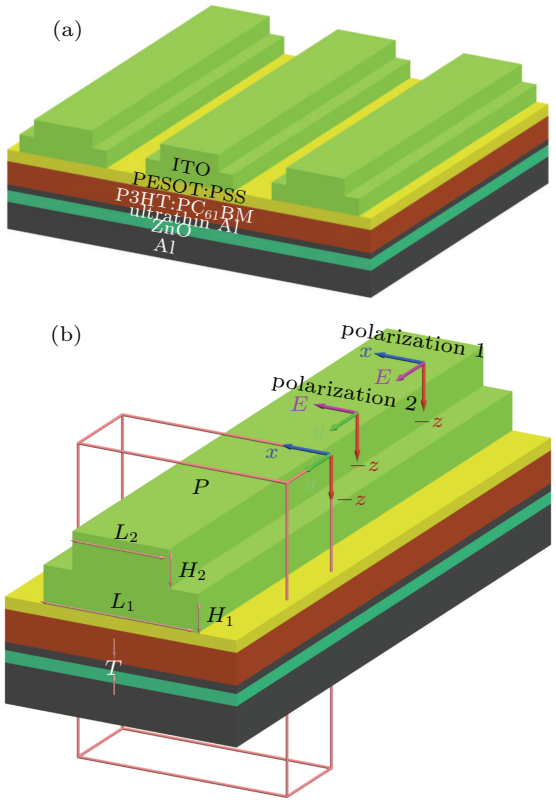


Fig. 1. (a) Schematized 3D structure of investigated devices, and (b) simulated minimum period structure.

Furthermore, the current density (J)–voltage (V) relation is calculated to more visually evaluate the device performance. The open-circuit voltage (V_{oc}) of the control device with a 160-nm-thick ITO planar layer and without the inserted Al layer is first estimated by the empirical formula[40]

$$V_{oc} = \frac{1}{e}(|E_{HOMO}^{Donor}| - |E_{LUMO}^{Acceptor}|) - 0.3\ \mathrm{V}, \tag{4}$$

where e is the elemental charge, E_{HOMO}^{Donor} and $E_{LUMO}^{Acceptor}$ are the energy levels of the highest occupied molecular orbital (HOMO) for the donor (P3HT, -5.2 eV) and the lowest unoccupied molecular orbital (LUMO) for the acceptor (PC_{61}BM, -4.2 eV), respectively, and 0.3 V is an empirical value

adopted in the relative study.[41,42] The values of J_{sc} and V_{oc} of the control device are then used to evaluate the saturation dark current density J from the following equation:[43]

$$J_0 = \frac{J_{sc}}{\exp(eV_{oc}/kT) - 1}, \tag{5}$$

where k is the Boltzmann constant, T is the absolute temperature, and 300 K is adopted in this study. Then the J–V curves for the devices with the proposed light management structure can be plotted from the following equation:

$$J(V) = J_0 \left[\exp(eV/kT) - 1\right]. \tag{6}$$

3. Results and discussion

Figures 2(a), 2(b), and 2(c) show the contour plots of J_{sc} as a function of L_1 and L_2/L_1, respectively, at P value of 200, 320, and 450 nm. It is evident that excellent light confinement can be achieved in a broad parameter range, thus providing convenience for fabricating the related high-performance devices. It is notable that a J_{sc} value of $\sim$ 12.14 mA/cm^2, *i.e.*, $>$ 72.0% absorption for the incident photons with energy larger than 1.9 eV, can be achieved for the device with P being 320 nm, and L_1 and L_2/L_1 around 180 nm and 0.611, respectively, as exhibited in Fig. 2(b) As a striking contrast, the control device with a 160-nm-thick flat ITO film only delivers the J_{sc} of $\sim$ 9.13 mA/cm^2, indicating the excellent light management for the proposed optical structure. Furthermore, it is noted that for a fixed L_1, J_{sc} normally decreases if L_2/L_1 is too large or small, and that the J_{sc} contour shifts towards higher L_1 as P increases.

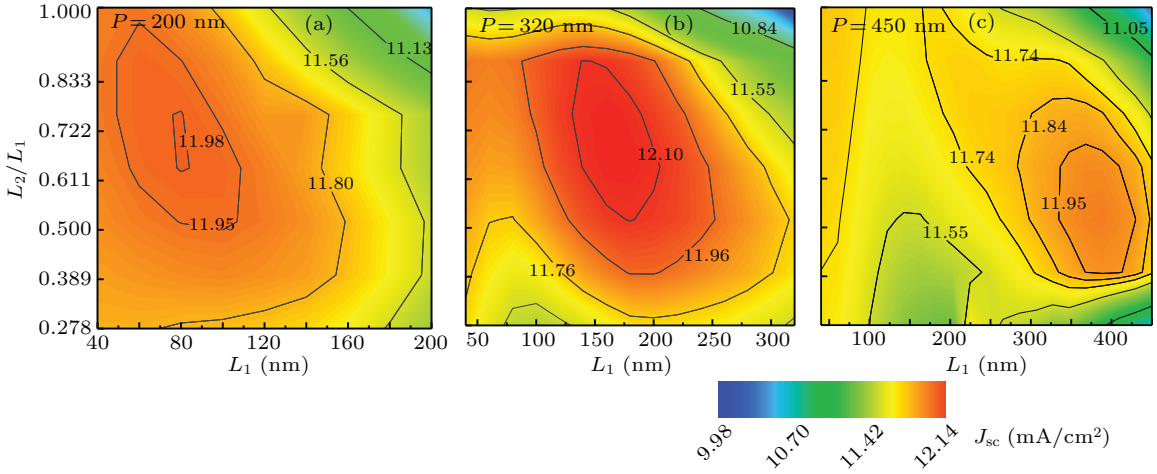


Fig. 2. Contour plots of J_{sc} as a function of L_1 and L_2/L_1 for P value of (a) 200, (b) 320, and (c) 450 nm, with thickness of the ultrathin Al layer being 5 nm.

To understand the mechanism of enhancing J_{sc} after applying the ITO nanograting, the optical behaviors of the device with the ITO nanograting are compared with those of the control device with a 160-nm-thick flat ITO layer. Figure 3(a) shows the light reflection spectra and $R_{in.}$ (inset) for the devices after introducing the nanograting structures with a P value of 320 nm, an $L_2/L_1$of 0.611 and different L_1 values of 80, 180, and 280 nm. It is evident that the light reflection is significantly suppressed especially in a spectral region from 400 nm to 650 nm as compared with the scenario of the control device. Accordingly, the light absorption of the photoactive layer in the corresponding spectral region (see Fig. 3(b)) and thus the J_{sc} can be enhanced for the ITO nanograting-incorporated device. Moreover, it is noted that for a fixed L_1, the light reflection is observed to increase if L_2/L_1 is too large or too small due to the destroyed continuity of the refractive index of the ITO nanograting as demonstrated by the reflection spectra and $R_{in.}$ (inset) in Fig. 3(c) It thus leads to the better light absorption as exhibited in Fig. 3(d) and the higher J_{sc} (see Fig. 2) of the photoactive layer for the modest L_2/L_1.

Besides the structural parameters of the ITO nanograting and the thickness of the ultrathin Al layer, T is found to have an evident influence on light absorption of the photoactive layer. As summarized in Table 1 for the device with P of 320 nm, and L_1 and L_2/L_1 of 180 nm and 0.611, the maximum J_{sc} can be predicted to be 12.14 mA/cm^2 that is 14.21% higher than that in the case without this thin Al layer, when T is around 5 nm. The further investigation indicates that the reduced light reflection (see Fig. 4) in the spectral region of 500 nm–600 nm in which the photon density is relatively high for the P3HT:PC_{61}BM blend can improve J_{sc} for the device with T of 5 nm as compared with the scenarios in other cases.

To more comprehensively understand light management of the proposed structure, influences of the optical structures, *i.e.* the ITO nanograting and 5-nm-thick ultrathin Al layer on the electric-field strength in the devices are investigated. Figure 5 shows the comparison between the distributions of the electric-field strength in the cross-section of the devices at two representative wavelengths of 420 nm and 580 nm. It is first noted that the electric-field strength in the photoactive layer

(see Figs. 5(a), 5(b), 5(e), and 5(f)) is evidently enhanced for the nanograting-incorporated structure ($P = 320$ nm, $L_1 = 180$ nm, $L_2/L_1 = 0.611$) because of the scattering effect on the incident light compared with the counterparts for the device without the nanograting (see Figs. 5(c), 5(d), 5(g), and 5(h)). Moreover, after introducing the 5-nm-thick Al layer between the photoactive layer and the electron transport layer, *i.e.* ZnO, the intensity of the electric field in ZnO is significantly suppressed as more clearly demonstrated in Fig. 6, thus reducing the corresponding energy loss.

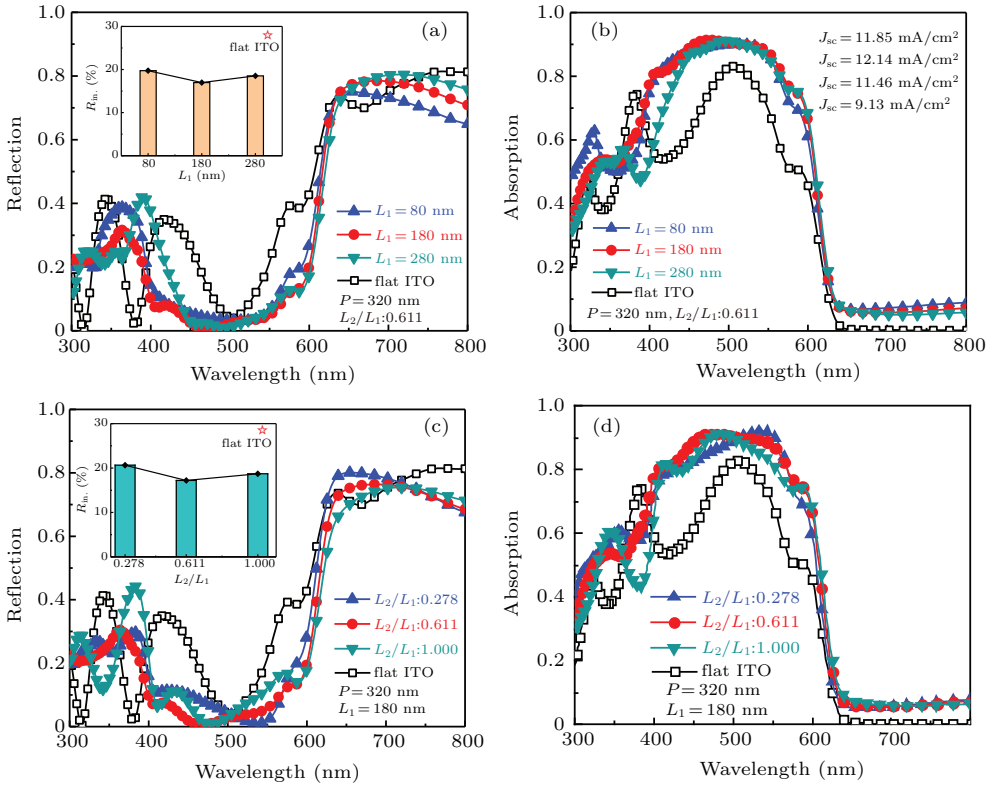


Fig. 3. (a) Reflection spectra and $R_{in.}$ (inset) for devices after introducing nanograting structures with P of 320 nm, L_2/L_1 of 0.611 and different L_1 values of 80, 180, and 280 nm, and (b) corresponding absorption spectra of photoactive layers, (c) reflection spectra and $R_{in.}$ (inset) for devices after introducing nanograting structures with P of 180 nm and L_2/L_1 values of 0.278, 0.611, and 1, and (d) corresponding absorption spectra of photoactive layers with corresponding data of the device with a 160-nm thick ITO film serving as reference.

Table 1. J_{sc} of devices with ultrathin Al layers with different thicknesses in between photoactive layer and ZnO ETL.

Thickness of ultrathin Al (nm)	1	3	5	7	9	w/o
J_{sc} (mA/cm^2)	11.44	11.79	12.14	11.78	11.47	10.63

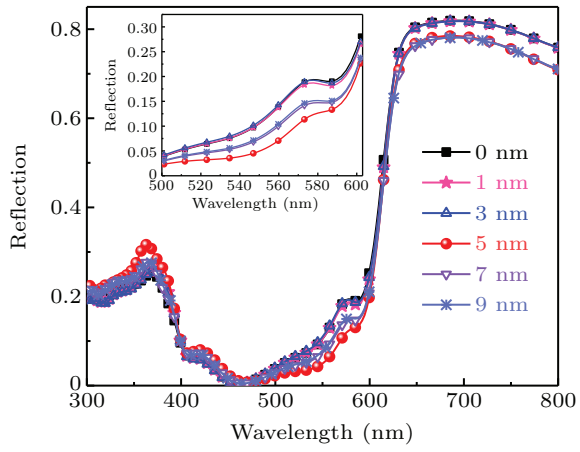


Fig. 4. Reflection spectra of devices with ITO nanograting of $P = 320$ nm, $L_1 = 180$ nm, $L_2/L_1 = 0.611$, and varying ultrathin Al layer thicknesses, with inset showing high-resolution reflection spectra between 500 nm and 600 nm.

For an excellent light management structure, it is vital to have efficient absorption even under oblique incidence. Owing to the reduced symmetry, the proposed structure should show better sensitivity to the incident plane. Accordingly, the absorption spectra at the incident angles of 0°, 30°, and 60° are exhibited for two representative cases with the incident plane *xz* (Fig. 7(a)) and incident plane *yz* (Fig. 7(b)). The ITO nanograting of $P = 320$ nm, $L_1 = 180$ nm, $L_2/L_1 = 0.611$ and the 5-nm-thick Al layer are adopted. It is evident that the light absorption with the incident plane *xz* is more sensitive to the incident angle as compared with that with the incident plane *yz*. Anyway, for both cases, the reduction of light absorption with the incident angle in a broad range of 0°–60° is limited, thus demonstrating the excellent light confinement for the proposed light management structure. The calculated J_{sc} at the incident angles of 0°, 30°, and 60° is respectively, 12.14, 10.07, and 5.45 mA/cm^2, showing limited reduction as compared with the corresponding value of 16.95, 14.68, and 8.47 mA/cm^2 for an ideal photoactive layer (100% absorption to the incident light). Significantly, the light utilization rate is still 64% even at 60°, which is much higher than 54% under normal incidence for the planar control device.

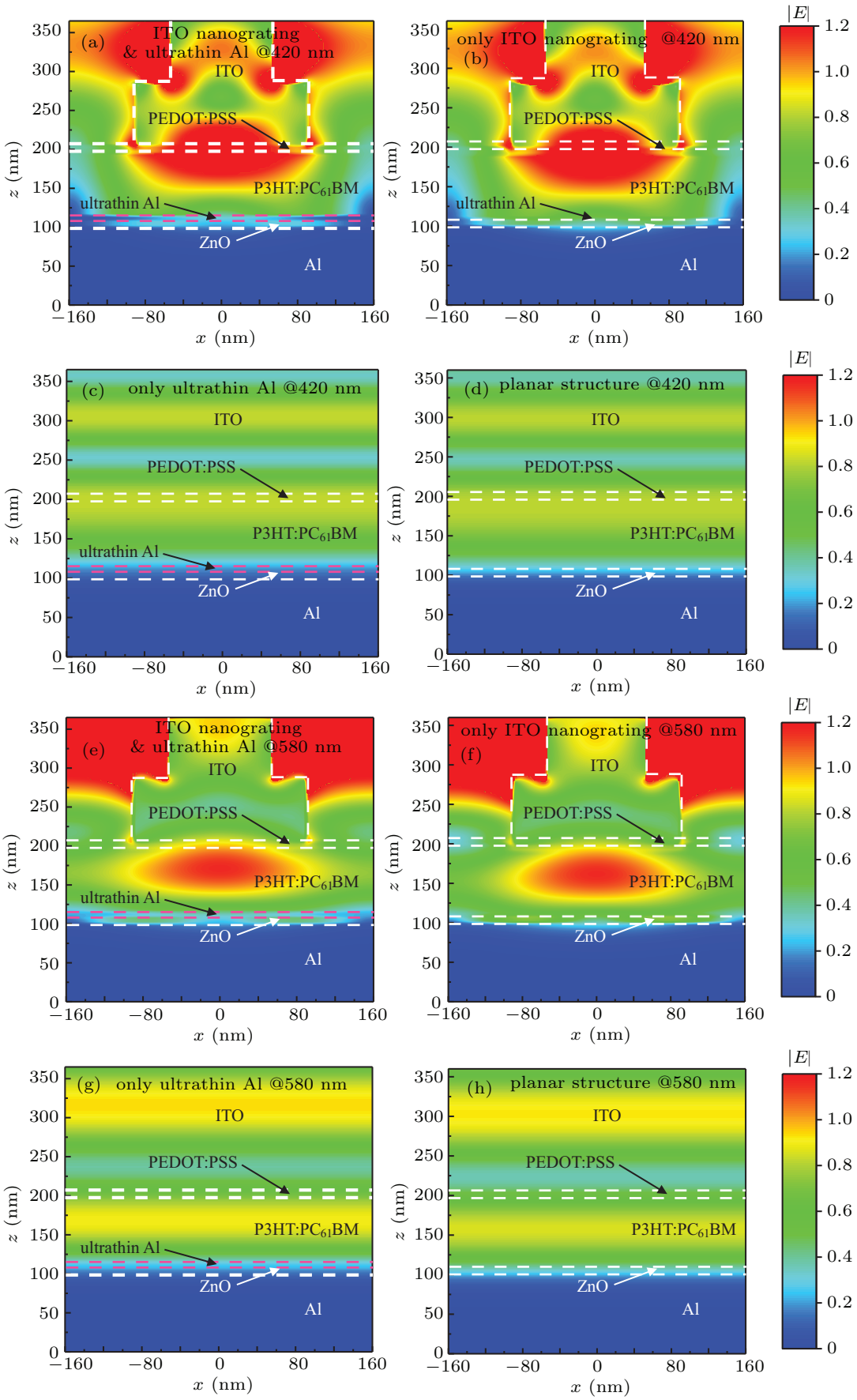


Fig. 5. Distributions of electric-field strength in cross-section of devices respectively [(a), (e)] with nanograting and 5-nm-thick Al layer in between photoactive layer and electron transport layer of ZnO at wavelength 420 nm and 580 nm, respectively, [(b), (f)] with nanograting but without 5-nm-thick Al layer at wavelength 420 nm and 580 nm, respectively, ((c), (g)) with the 160-nm-thick ITO planar layer and 5-nm-thick Al layer at wavelength 420 nm and 580 nm, respectively, [(d) (h)] with only 160-nm-thick ITO planar layer at wavelength 420 nm and 580 nm, P, L_1, and L_2/L_1 of 320 nm, 180 nm, and 0.611, respectively.

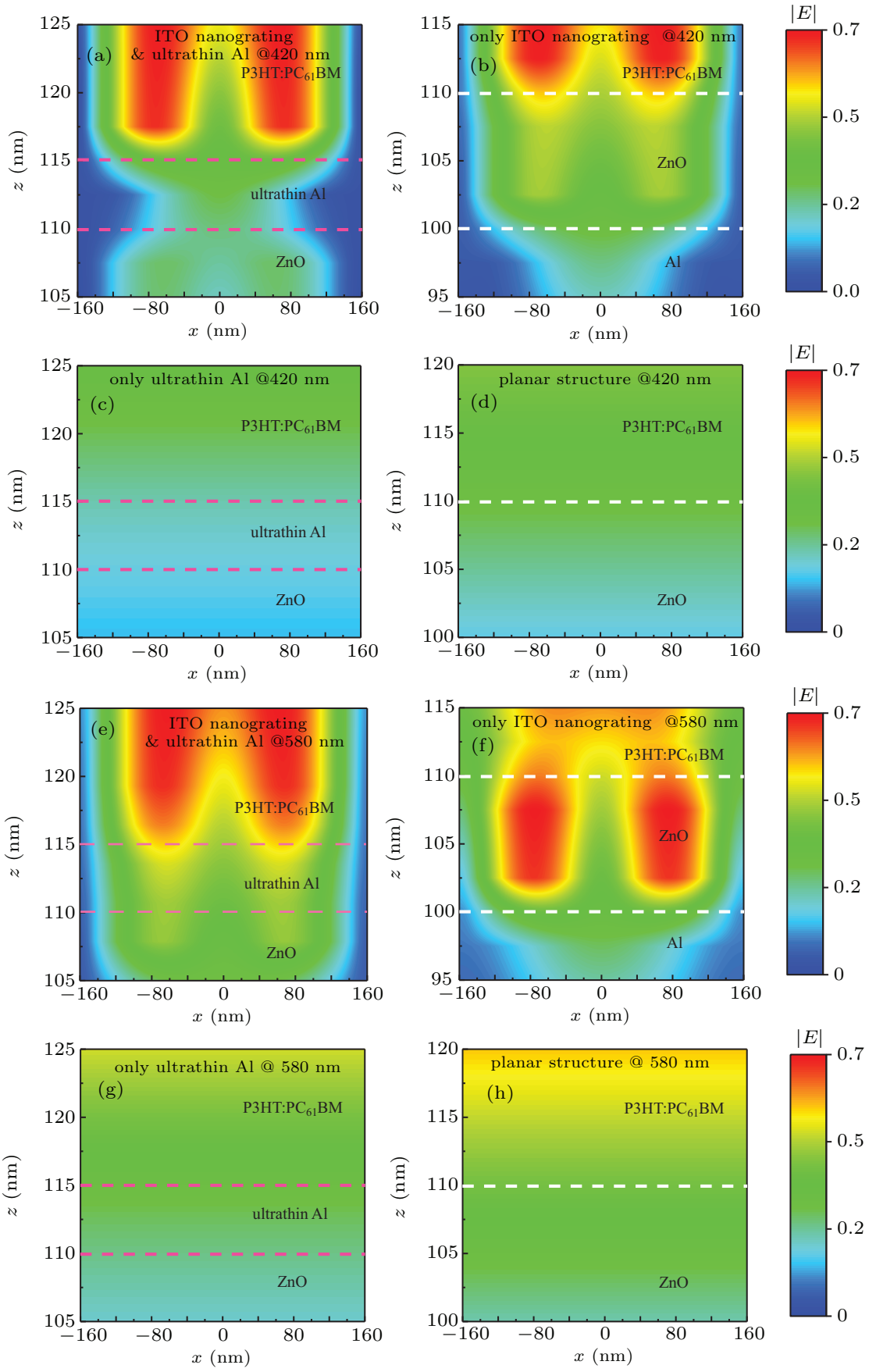


Fig. 6. Distributions of electric-field strength in cross-section of devices in the vicinity of ultrathin Al layer or interface between photoactive layer and ZnO: [(a), (e)] with nanograting and 5-nm-thick Al layer in-between photoactive layer and electron transport layer of ZnO at wavelength 420 nm and 580 nm, respectively, [(b), (f)] with nanograting but without 5-nm-thick Al layer at 420 and 580 nm, respectively, [(c), (g)] with wavelength 160-nm ITO planar layer and 5-nm-thick Al layer at wavelength 420 nm and 580 nm, respectively, [(d), (h)] with only 160-nm-thick ITO planar layer at wavelength of 420 nm and 580 nm, P, L_1, and L_2/L_1 are 320 nm, 180 nm, and 0.611, respectively.

Table 2. Device parameters extracted from the *J*–*V* curves in Fig. 8.

Device	J_{sc} (mA/cm^2)	V_{oc} (V)	FF (%)	PCE (%)	PCE (%) @ FF of 60%
Control device	9.13	0.700	84.57	5.40	3.83
ITO nanograting	10.63	0.704	84.63	6.33	4.50
ITO nanograting +5-nm ultrathin Al	12.14	0.707	84.68	7.27	5.15
Ideal absorber	16.95	0.716	84.81	10.29	6.17

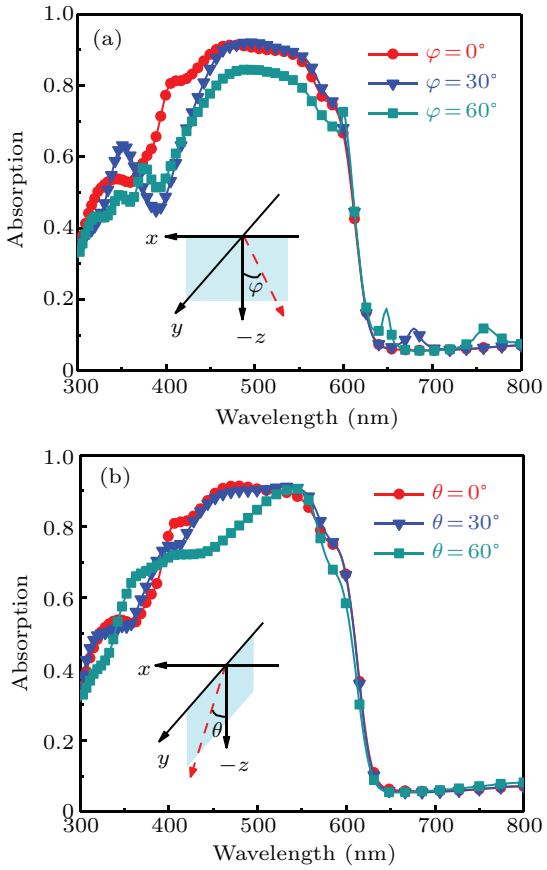


Fig. 7. Light absorptions of photoactive layer in device with nanograting of $P = 320$ nm, $L_1 = 180$ nm, $L_2/L_1 = 0.611$ and 5-nm-thick ultrathin Al layer for light with (a) incident plane of *xz* and (b) incident plane *yz* at incident angles of 0°, 30°, and 60°, respectively.

Figure 8 exhibits the calculated *J*–*V* curves at AM 1.5G illumination for the devices with only the ITO nanograting ($P = 320$ nm, $L_1 = 180$ nm, $L_2/L_1 = 0.611$), and with both ITO nanograting and 5-nm-thick Al layer in between the photoactive layer and the ZnO, together with a control device with a 160-nm-thick ITO layer, and the device with an ideal P3HT:$PC_{61}BM$ absorber, *i.e.* 100% light absorption. The key device parameters, including J_{sc}, V_{oc}, fill factor (FF) PCE extracted from the *J*–*V* curves, and the PCE estimated assuming FF = 60%[44,45] are summarized in Table 2. It is observed that the PCE of the device with an optimal light management structure is significantly improved compared with that of the control device because of the enhanced J_{sc}.

Finally, the PTB7:$PC_{71}BM$ layer[46,47] is employed to evaluate the feasibilities of the proposed light management structure for other photoactive layers. Figure 9 shows the light absorption spectra of the 100-nm-thick PTB7:$PC_{71}BM$ layers for the device with and without the light management structure, *i.e.*, the ITO nanograting ($P = 320$ nm, $L_1 = 180$ nm, and $L_2/L_1 = 0.611$) and the 5-nm-thick ultrathin Al, under the normal incidence. It is evident that comparing with the control device, the light absorption of the photoactive layer is remarkably enhanced after incorporating the light management structure, leading to 22.47% increment of J_{sc}, *i.e.*, from 15.13 mA/cm^2 to 18.53 mA/cm^2.

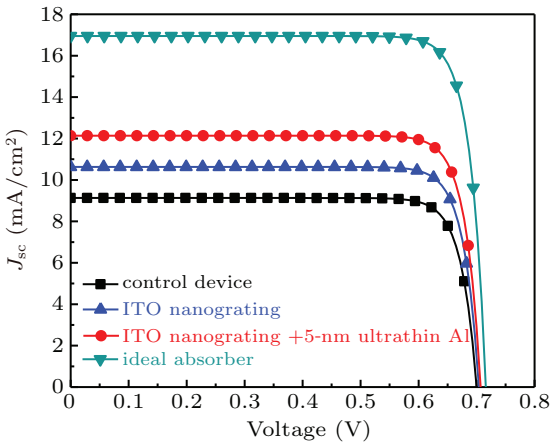


Fig. 8. Calculated *J*–*V* curves at AM 1.5G illumination.

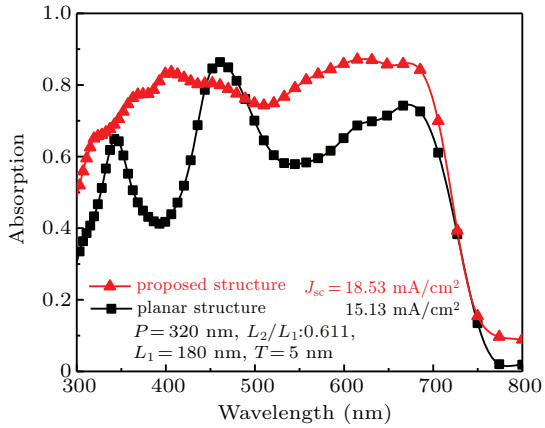


Fig. 9. Light absorption of 100-nm-thick PTB7:$PC_{71}BM$ layer for the device with and without optimal light management structure.

4. Conclusions

In this paper, we introduce a simple light management structure consisting of a front ITO nanograting and ultrathin Al layer inserted in between the photoactive layer and the ETL, which is applicable to thin film-based optoelectronic devices. Owing to the synergetic effects including antireflection and

light scattering by the nanograting and suppressed light absorption of the ETL by the inserted Al layer, the light absorption of the photoactive layer can be remarkably enhanced in a broad parameter range of the nanograting, and thus provides the convenience for fabricating the relevant devices. Furthermore, it is found that compared with the control device with a planar configuration of ITO/PEDOT:PSS/P3HT:$PC_{61}BM$ (80-nm thick)/ZnO/Al, J_{sc} and PCE can be improved by 32.86% and 34.46% after introducing the optimized light management structure, *i.e.*, the ITO nanograting of $P = 320$ nm, $L_1 = 180$ nm, $L_2/L_1 = 0.611$, and 5-nm-thick Al layer. In addition, the proposed device structure exhibits good omnidirectional light management and feasibility for other photoactive materials. Owing to the simple structure and excellent performance, we believe that this work provides valuable exploration of light management structures for thin film-based optoelectronic devices.

References

[1] An Q, Zhang F, Zhang J, Tang W, Deng Z and Hu B 2016 *Energy Environ. Sci.* **9** 281

[2] Lu C, Yan P, Wang J, Liu A, Song D and Jiang C 2014 *Chin. Phys. B* **23** 088803

[3] Xiao X, Yi N, Yao G, Lu J, Leng S, Hu M, Yuan Z and Zhou W 2020 *ACS Appl. Mater. Interfaces* **12** 58082

[4] Li J, Yu H, Wong S M, Li X, Zhang G, Lo P G Q and Kwong D L 2009 *Appl. Phys. Lett.* **95** 243113

[5] Ali B A, Moubah R, Boulezhar A and Lassri H 2020 *Chin. Phys. B* **29** 098801

[6] Chen J T and Hsu C S 2011 *Polym. Chem.* **2** 2707

[7] Wang Y, Shao P, Chen Q, Li Y, Li J and He D 2017 *J. Phys. D: Appl. Phys.* **50** 175105

[8] Wu Z, Wang Y, Zhang Y, Zhang W, Liu Q, Liu Q, Chen Q, Li Y, Li J and He D 2019 *Org. Electron.* **73** 7

[9] Shi W, Kan Z, Cheng C, Li W, Song H, Li M, Yu D, Du X, Liu W, Jin S and Cong S 2020 *Chin. Phys. Lett.* **37** 108401

[10] Xiang C, Jin Y, Liu J, Xu B, Wang W, Wei X, Song G and Xu Y 2014 *Chin. Phys. B* **23** 038803

[11] Cui Y, Yao H, Zhang J, Xian K, Zhang T, Hong L, Wang Y, Xu Y, Ma K, An, C, He C, Wei Z, Gao F and Hou J 2020 *Adv. Mater.* **32** 1908205

[12] Huang H, Tian G, Zhou L, Yuan J, Fahrner W R, Zhang W, Li X, Chen W and Liu R 2018 *Chin. Phys. B* **27** 038502

[13] In S, Mason D R, Lee H, Jung M, Lee C and Park N 2015 *ACS Photon.* **2** 78

[14] Wang Y, Zhang Y, Zhang L, Wu Z, Su Q, Liu Q, Fu Y, Li J, Li Y and He D 2020 *Mater. Chem. Phys.* **254** 123536

[15] Lehr J, Mertens A, Liu Q, Martorell J, Paetzold U W and Lemmer U 2020 *Opt. Express* **28** 37986

[16] Chen Y, Li L, Liu Z, Zhou N, Chen Q and Zhou H 2017 *Nano Energy* **40** 540

[17] Li Y, Gao P, Chen Q, Yang J, Li J and He D 2016 *J. Phys. D: Appl. Phys.* **49** 215104

[18] Fang H, Li X, Song S, Xu Y and Zhu J 2008 *Nanotechnology* **19** 255703

[19] Song Y, Zhang Y, Song J, Li K, Zhang Z, Xu Y, Song G and Chen L 2015 *Chin. Phys. Lett.* **32** 074206

[20] Li J, Yu H, Wong S M, Zhang G, Sun X, Lo P G Q and Kwong D L 2009 *Appl. Phys. Lett.* **95** 033102

[21] Li H, Hu Y, Wang Y and Zhu F 2020 *Sol. Energy Mater. Sol. Cells* **211** 110529

[22] Chen X, Wang J, Shao P, Liu Q, Liu D, Chen Q, Li Y, Li J and He D 2018 *Nanoscale Res. Lett.* **13** 236

[23] Li J, Hu H and Li Y 2012 *Nanotechnology* **23** 194010

[24] Li J, Yu H and Li Y, Wang F, Yang M and Wong S M 2011 *Appl. Phys. Lett.* **98** 021905

[25] Calvo M and H.M 2015 *J. Phys. Chem. C* **119** 18635

[26] Park Y, Vandewal K and Leo K 2018 *Small Methods* **2** 1800123

[27] Jiang Z, Hu D, Pang L, Gao F and Wang P 2018 *Chin. Phys. B* **27** 054201

[28] Cai B, Li X, Zhang Y and Jia B 2016 *Nanotechnology* **27** 195401

[29] Gao P, Wang H, Sun Z, Han W, Li J and Ye J 2013 *Appl. Phys. Lett.* **103** 253105

[30] Lim E L, Yap C C, Teridi M A M, Teh C H, Yusoff A R M and Jumali M H H 2016 *Org. Electron.* **36** 12

[31] Wang R, Gong Q and Chen J 2020 *Chin. Phys. B* **29** 064215

[32] Qu D, Liu F, Huang Y, Xie W and Xu Q 2011 *Opt. Express* **19** 24795

[33] Yang J, Zhang P, Wang J and Wei S H 2020 *Chin. Phys. B* **29** 108401

[34] Li Y, Wang J, Zhang W, Liu Q, Chen Q and Li J 2019 *J. Phys. D: Appl. Phys.* **52** 435501

[35] Shen P, Wang G, Kang B, Guo W, and Shen L 2018 *ACS Appl. Mater. Interfaces* **10** 6513

[36] Shin D H, Jang C W, Ko J S, and Choi S H 2021 *Appl. Surf. Sci.* **538** 148155

[37] Sandhu S, Yu Z and Fan S 2015 *J. Phys. D: Appl. Phys.* **48** 413001

[38] Li L, Shi C, Deng X, Wang Y, Xiao G, Ni L 2018 *Chin. Phys. B* **27** 018804

[39] Zhang Y, Cui Y, Wang W, Fung K H, Ji T, Hao Y and Zhu F 2015 *Plasmonics* **10** 773

[40] Kumar K, Kumamat U K, Mital R, and Dhawaw A 2019 *J. Opt. Soc. Am. B* **36** 978

[41] Wu Z, Zhang W, Xie C, Zhang L, Wang Y, Zhang Y, Liu Q, Fu Y, Li Y, Li J and He D 2020 *IEEE J. Photovolt.* **10** 1353

[42] Shao P, Chen X, Guo X, Zhang W, Chang F, Liu Q, Chen Q, Li J, Li Y and He D 2017 *Org. Electron.* **50** 77

[43] Hegedus S S, and Shafarman W N 2004 *Prog. Photovolt: Res. Appl.* **12** 155

[44] Huang S, Tang Y, Dang Y, Xu X, Dong Q, Kang B and Silva P P S R 2018 *ACS Sustain. Chem. Eng.* **6** 6702

[45] Trana V H, Eomc S H, Yoonc S C, Kimb S K and Leeb S H 2019 *Org. Electron.* **68** 85

[46] Kniepert J, Lange I, Heidbrink J, Kurpiers J, Brenner T J K, Koster L J A and Neher D 2015 *J. Phys. Chem. C* **119** 8310

[47] Zheng Y, Wang G, Huang D, Kong J, Goh T, Huang W, Yu J S and Taylor A D 2018 *Sol. RRL* **2** 1700144